Simultaneous Control of Morphology and Porosity in Nanoporous Carbon: Graphitic Mesoporous Carbon Nanorods and Nanotubules with Tunable Pore Size

Yongde Xia, Zhuxian Yang, and Robert Mokaya*

School of Chemistry, University of Nottingham, University Park, Nottingham NG7 2RD, U.K.

Received October 12, 2005. Revised Manuscript Received November 8, 2005

We report on the use of simple chemical vapor deposition (CVD) nanocasting routes to simultaneously control the morphology, pore size, and graphitization in structurally well-ordered mesoporous carbons. Mesoporous silica SBA-15 rods were used as hard templates to nanocast mesostructured carbon nanorods and nanotubules with tunable pore size. The pore size of the carbons was tunable between 2 and 4.5 nm by simply using SBA-15 silica templates synthesized at various temperatures between 40 and 130 °C. Depending on the textural properties (and in particular the pore size) of the SBA-15 silica template, the particle morphology of the mesoporous carbon materials was changeable from nanorods (solid core) to hollow nanotubules. Small-pore SBA-15 silicas resulted in mesoporous carbon hollow tubes (nanotubules), whereas larger-pore silicas yielded solid-core rods. The nature of the SBA-15 silica did not affect the extent of graphitization. Greater levels of graphitization were, however, obtained for carbons prepared at higher CVD temperatures. To the best of our knowledge, this is the first successful attempt to control both the morphology and pore size of graphitic mesoporous carbons. Furthermore, this study demonstrates a new concept in which the pore size of the silica template plays a key role in directing the morphology of templated mesoporous carbon toward hollow particles (nanotubules) rather than solid-core particles (nanorods).

1. Introduction

In recent years, well-ordered mesoporous carbon materials have attracted increasing attention because of their potential use in gas storage or as molecular sieves, catalyst supports, electrode materials, templates, or nanoreactors.[1−3] Generally, mesoporous carbon materials are fabricated via sacrificial solid templating approaches in which mesoporous silicas or aluminosilicas are infiltrated with carbon precursors and then subjected to carbonization at high temperature and finally selective removal of the inorganic templates.[4−6] Various forms of mesoporous silicas and aluminosilicas, including MCM-48, SBA-15, HMS, MSU-H, SBA-12, SBA-16, and mesocelluar silica foams, have been used as sacrificial templates for the preparation of mesoporous carbons.[4−6] The pore channel system of mesoporous carbons is usually inversely replicated from the inorganic templates, and in general, the carbons retain the particle morphology of the template.[4−8] Therefore, to prepare mesoporous carbon materials with particular porosity and/or morphology, it is necessary to control the textural properties and particle morphology of the inorganic templates.[7,8] The morphology of ordered mesostructured carbons is an important factor in their use as catalysts, as molecular sieves, or as hosts for occlusion compounds in composite materials for advanced applications.[2,3] In addition to morphology, the porosity, particularly the pore diameter of mesoporous carbon materials, is another key physical parameter. The ability to finely control the porosity and pore size of mesoporous carbons is a desirable research goal that has not been fully explored. Indeed, there are only a few reported attempts to finely control the porosity of mesoporous carbons. Attempts to vary the pore size of mesoporous carbons have so far resulted in either modest pore size ranges[7,9] or bimodal pore systems with large (>8 nm) pore diameters.[10]

Another desirable property in nanoporous carbons is a graphitic framework, which enhances the thermal stability

* Corresponding author. E-mail: r.mokaya@nottingham.ac.uk.

(1) (a) Dillon, A. C.; Jones, K. M.; Bekkedahl, T. A.; Kiang, C. H.; Bethune, D. S.; Heben, M. J. *Nature* **1997**, *386*, 377. (b) Kyotani, T. *Carbon* **2000**, *38*, 269. (c) Kang, M.; Yi, S. H.; Lee, H. I.; Yie, J. E.; Kim, J. M. *Chem. Commun.* **2002**, 1944. (d) Yang, Z.; Xia, Y.; Mokaya, R. *Adv. Mater.* **2004**, *16*, 727.

(2) (a) Ryoo, R.; Joo, S. H.; Kruk, M.; Jaroniec, M. *Adv. Mater.* **2001**, *13*, 677. (b) Lee, J.; Han, S.; Hyeon, T. *J. Mater. Chem.* **2004**, *14*, 478.

(3) Yang, H. F.; Zhao, D. Y. *J. Mater. Chem.* **2005**, *15*, 1217.

(4) (a) Ryoo, R.; Joo, S. H.; Jun, S. *J. Phys. Chem. B* **1999**, *103*, 7743. (b) Jun, S.; Joo, S. H.; Ryoo, R.; Kruk, M.; Jaroniec, M.; Liu, Z.; Ohsuna, T.; Terasaki, O. *J. Am. Chem. Soc.* **2000**, *122*, 10712. (c) Lee, J.; Yoon, S.; Hyeon, T.; Oh, S. M.; Kim, K. B. *Chem. Commun.* **1999**, 2177.

(5) Kruk, M.; Dufour, B.; Celer, E. B.; Kowalewski, T.; Jaroniec, M.; Matyjaszewski, K. *J. Phys. Chem. B* **2005**, *109*, 9216.

(6) (a) Lu, A.; Kiefer, A.; Schmidt, W.; Schueth, F. *Chem. Mater.* **2004**, *16*, 100. (b) Alvarez, S.; Fuertes, A. B. *Carbon* **2004**, *42*, 433. (c) Tian, B.; Che, S.; Liu, Z.; Liu, X.; Fan, W.; Tatsumi, T.; Terasaki, O.; Zhao, D. *Chem. Commun.* **2003**, 2726. (d) Fuertes, A. B. *J. Mater. Chem.* **2003**, *13*, 3085. (e) Lee, J.; Sohn, K.; Hyeon, T. *J. Am. Chem. Soc.* **2001**, *123*, 5146. (f) Kim, S.-S.; Pinnavaia, T. J. *Chem. Commun.* **2001**, 2418. (g) Lee, J.; Yoon, S.; Oh, S. M.; Shin, C.-H.; Hyeon, T. *Adv. Mater.* **2000**, *12*, 359.

(7) (a) Yu, C.; Fan, J.; Tian, B.; Zhao, D.; Stucky, G. D. *Adv. Mater.* **2002**, *14*, 1742. (b) Yu, C.; Fan, J.; Tian, B.; Zhang, F.; Stucky, G. D.; Zhao, D. *Stud. Surf. Sci. Catal.* **2003**, *146*, 45.

(8) (a) Xia, Y.; Mokaya, R. *Adv. Mater.* **2004**, *16*, 886. (b) Xia, Y. D.; Yang, Z. X.; Mokaya, R. *J. Phys. Chem. B* **2004**, *108*, 19293. (c) Xia, Y.; Yang, Z.; Mokaya, R. *Stud. Surf. Sci. Catal.* **2005**, *156*, 565.

10.1021/cm0522634 CCC: $33.50
Published on Web 12/10/2005

and electrical conductivity. In general, mesoporous carbon materials obtained via sacrificial hard template approaches contain amorphous pore walls.[4−7,9,10] Recently, the groups of Ryoo and Pinnavaia synthesized partially graphitic mesoporous carbons via in situ conversion of aromatic compounds into mesophase pitch in the pores of mesoporous aluminosilicates.[11,12] Other groups have independently reported that graphitic mesoporous carbon can be prepared using pitches as the carbon source and colloid or mesoporous silicas as the solid templates.[13,14] Fuertes and Centeno synthesized partially graphitic mesoporous carbon via the polymerization of pyrrole in mesoporous silicas impregnated with $FeCl_3$.[15] We, on the other hand, have recently found that graphitic mesoporous carbon materials that display a variety of particle morphologies, including hollow spheres, can be readily fabricated via simple noncatalytic chemical vapor deposition (CVD).[16] Here, we report on our attempts to use CVD nanocasting to control the morphology, pore size, and graphitization in mesoporous carbons. We have used mesoporous silica SBA-15 rods to nanocast graphitic mesostructured carbon nanorods and nanotubules with a tunable pore size via a simple CVD route. This method allows the simultaneous control of both the morphology and the pore size of *graphitic* mesoporous carbons. We also show that, depending on the nature (textural properties) of the silica template, the particle morphology of the carbon materials was changeable from nanorods (solid core) to hollow nanotubules. The findings on pore-size-dependent control of morphology offer new opportunities to tailor the morphology of mesoporous carbons toward hollow particles.

2. Experimental Section

2.1. Material Synthesis. The SBA-15 rod templates were prepared following a previous report.[17] Typically, 4.0 g of triblock copolymer poly(ethylene glycol)-*block*-poly(propylene glycol)-*block*-poly(ethylene glycol) ($EO_{20}PO_{70}EO_{20}$) was added into a solution of 120 g of 2 M HCl and 30 g of water. After being continuously stirred at 40 °C overnight, 8.6 g of TEOS was added to the solution. Following continuous stirring for 5 min at 40 °C, the reaction mixture was transferred to a Teflon-lined autoclave and heated at 40 °C for 20 h first and then at a temperature between 40 and 130 °C for 24 h. The resulting product was obtained by filtration, washed repeatedly with a large amount of water, air-dried at room temperature, and calcined at 500 °C for 6 h to remove the surfactant. The obtained SBA-15 samples were labeled as RSBA15-*X*, where *X* is the final crystallization temperature. The calcined SBA-15 silicas were used as templates for the preparation of mesoporous carbon via CVD. Typically, 0.3 g of calcined SBA-15 rods was placed in an alumina boat and inserted into a flow-through tube furnace in a fume cupboard. Under a flow of nitrogen saturated with acetonitrile vapor at room temperature, the temperature of the furnace was increased, at a ramp rate of 20 °C/min, to the final pyrolysis/carbonization temperature (in the range 900−1000 °C) and maintained at this temperature for 3 h under the acetonitrile-saturated nitrogen atmosphere. (*Caution: Hot organic vapors must be handled carefully!*) The furnace was then cooled to room temperature, and the resulting SBA-15/carbon mesophase thoroughly washed with hydroflouric (HF) acid to etch out the silica. (*Caution: HF acid is highly corrosive and must be handled with care!*) The resulting carbon materials were designated as RCMK3-*X*-*Y*, where *X* is the final crystallization temperature of the SBA-15 template and *Y* is the CVD temperature. The nitrogen content of the materials, determined using a CHNS analyzer (Fishons EA 1108), was between 6 and 8 wt %. X-ray photoelectron spectroscopy (XPS) indicated that the nitrogen was incorporated into the carbon framework as previously reported.[8,16]

2.2. Material Characterization. Powder XRD analysis was performed using a Philips 1830 powder diffractometer with Cu Kα radiation (40 kV, 40 mA). Nitrogen sorption isotherms and textural properties were determined at −196 °C using nitrogen in a conventional volumetric technique by an ASAP 2020 micrometrics sorptometer. Before analysis, the samples were oven dried at 150 °C and evacuated for 12 h at 200 °C under vacuum. The surface area was calculated using the BET method based on adsorption data in the partial pressure (P/P_0) range 0.05−0.2, and total pore volume was determined from the amount of the nitrogen adsorbed at $P/P_0 \approx 0.99$. Micropore surface area and micropore volume were obtained via *t*-plot analysis. Scanning electron microscopy (SEM) images were recorded using a JEOL JSM-820 scanning electron microscope. TEM images were recorded on a JEOL 2000-FX electron microscope operating at 200 kV. Thermogravimetric analysis (TGA) was performed using a Perkin-Elmer Pyris 6 TG analyzer at a heating rate of 2 °C/min under static air conditions.

3. Results and Discussion

3.1. Mesoporous Silica SBA-15 Templates. Mesoporous silica SBA-15 templates were prepared using a method that optimized the formation of rod particles.[17] The mesostructural ordering and pore size distribution of the silica templates was confirmed by nitrogen sorption analysis. Figure 1 shows the nitrogen sorption isotherms and corresponding pore size distributions for SBA-15 samples synthesized at various crystallization temperatures. All of the SBA-15 samples exhibit a type IV isotherm with a typical capillary condensation step into uniform mesopores in the partial pressure (P/P_0) range of 0.45−0.85. With an increase in the synthesis temperature from 40 to 130 °C, the capillary condensation step shifts to higher partial pressure, implying an increase in pore size. The textural properties of the silicas (Table 1) are typical for SBA-15-type materials. The textural properties therefore confirmed the suitability of the mesoporous silica SBA-15 rods for use as solid templates in the nanocasting of mesostructured carbon. The particle morphology of the SBA-15 silica templates was confirmed, as shown by the SEM images in Figure 2, to be uniform straight rods with diameters of 100−400 nm and lengths between 1 and 2 μm.[17]

(9) (a) Lee, J. S.; Joo, S. H.; Ryoo, R. *J. Am. Chem. Soc.* **2002**, *124*, 1156. (b) Vinu, A.; Ariga, K. *Chem. Lett.* **2005**, *34*, 674.
(10) (a) Lu, A.-H.; Schmidt, W.; Spliethoff, B.; Schueth, F. *Adv. Mater.* **2003**, *15*, 1602. (b) Lu, A. H.; Li, W. C.; Schmidt, W.; Schuth, F. *Microporous Mesoporous Mater.* **2005**, *80*, 117.
(11) Kim, T.-W.; Park, I.-S.; Ryoo, R. *Angew. Chem., Int. Ed.* **2003**, *42*, 4375.
(12) Kim, C. H.; Lee, D.-K.; Pinnavaia, T. J. *Langmuir* **2004**, *20*, 5157.
(13) (a) Yoon, S. B.; Chai, G. S.; Kang, S. K.; Yu, J. S.; Gierszal, K. P.; Jaroniec, M. *J. Am. Chem. Soc.* **2005**, *127*, 4188. (b) Li, Z.; Jaroniec, M.; Lee, Y.-J.; Radovic, L. R. *Chem. Commun.* **2002**, 1346. (c) Li, Z.; Jaroniec, M. *J. Phys. Chem. B* **2004**, *108*, 824.
(14) Yang, H. F.; Yan, Y.; Liu, Y.; Zhang, F. Q.; Zhang, R. Y.; Meng, Y.; Li, M.; Xie, S. H.; Tu, B.; Zhao, D. Y. *J. Phys. Chem. B* **2004**, *108*, 17320.
(15) Fuertes, A. B.; Centeno, T. A. *J. Mater. Chem.* **2005**, *15*, 1079.
(16) (a) Xia, Y. D.; Mokaya, R. *Adv. Mater.* **2004**, *16*, 1553. (b) Xia, Y. D.; Mokaya, R. *Chem. Mater.* **2005**, *17*, 1553.
(17) Sayari, A.; Han, B. H.; Yang, Y. *J. Am. Chem. Soc.* **2004**, *126*, 14348.

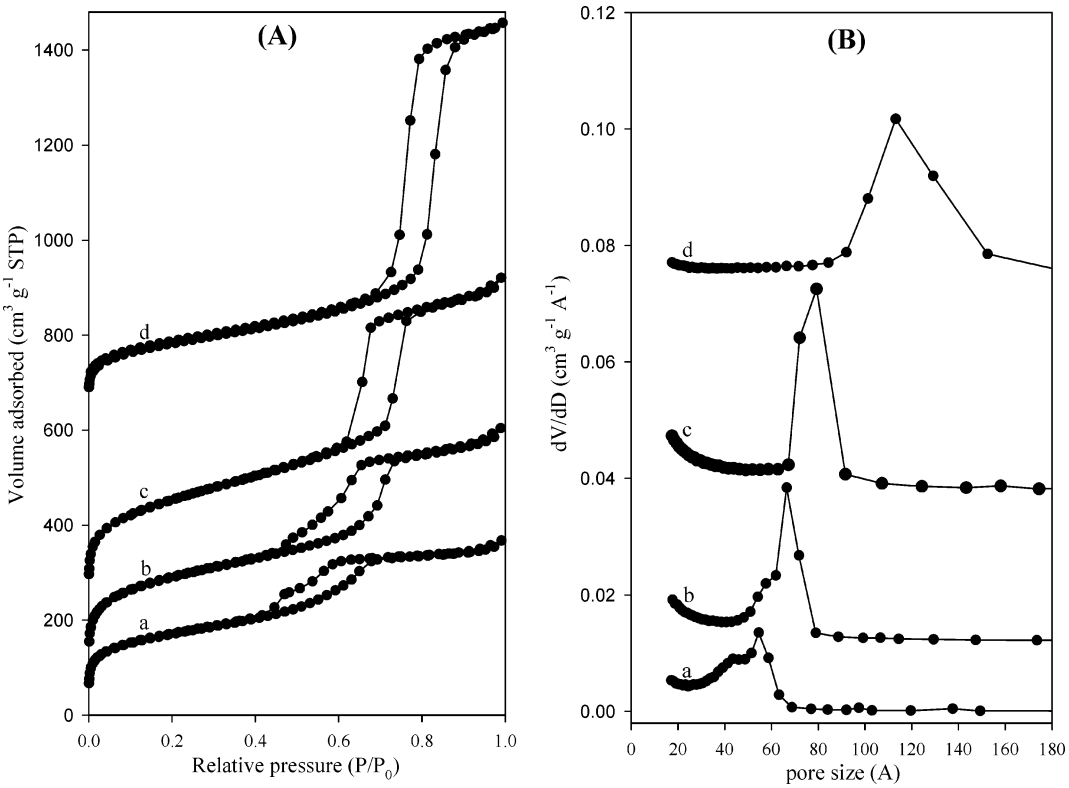

Figure 1. (A) Nitrogen sorption isotherms and (B) pore size distribution curves for mesoporous silica SBA-15 silica rods synthesized at various temperatures: (a) 40 °C (RSBA15-40), (b) 70 °C (RSBA15-70), (c) 100 °C (RSBA15-100), and (d) 130 °C (RSBA15-130). For clarity, isotherms b−d are offset (*y* axis) by 70, 230, and 650, respectively, and curves b−d are offset (*y* axis) by 0.012, 0.038, and 0.075, respectively.

Table 1. Textural Properties of Mesoporous Silica SBA-15 Rods (RSBA15) and Mesoporous Carbon Materials (RCMK3) Nanocast via Chemical Vapor Deposition Using Silica Rods as the Template

sample	surface area[a] (m^2/g)	pore volume[a] (cm^3/g)	pore size[b] (nm)
RSBA15-40	597 (194)	0.57 (0.09)	5.4
RSBA15-70	775 (229)	0.83 (0.10)	6.6
RSBA15-100	800 (143)	1.07 (0.06)	7.9
RSBA15-130	475 (72)	1.25 (0.03)	11.3
RCMK3-100-900	618 (0)	0.70 (0)	3.2
RCMK3-100-950	523 (0)	0.61 (0)	3.3
RCMK3-100-1000	340 (0)	0.41 (0)	3.1
RCMK3-40-950	278 (0)	0.40 (0)	2.1
RCMK3-70-950	414 (0)	0.50 (0)	2.8
RCMK3-130-950	386 (0)	0.46 (0)	4.1

[a] Data in parentheses are contributions from micropores. [b] Pore size was calculated by BJH analysis of the adsorption isotherm.

3.2. Effect of CVD Temperature on Structural Ordering and Graphitization of Carbon. The SBA-15 rods were used as templates to nanocast carbons via CVD. We first ascertained the effect of CVD temperature on structural ordering and graphitization of the resulting carbons. This was achieved by preparing carbons at a range of CVD temperatures (900, 950, and 1000 °C) using the 100 °C silica (RSBA15-100) as the template. Figure 3 shows the powder XRD patterns and nitrogen sorption isotherms for the resulting (RCMK3-100) carbons. All of the XRD patterns exhibit several low-angle diffractions; the basal (d_{100}) peak and at least one other peak. The resolution and intensity of the XRD peaks decreases for carbons prepared at higher CVD temperatures. It is also noticeable that the position of the basal peak shifts to higher 2θ values for carbons prepared at higher CVD temperatures, suggesting a reduction in basal spacing. The basal spacings derived from the XRD patterns are 9.17, 8.86, and 7.01 nm for carbons prepared at 900, 950, and 1000 °C, respectively. Apart from the basal (100) diffraction, the other low-angle peaks can be ascribed to (110), (200), and (210) diffractions from a hexagonal (*P*6*mm*) array of pores.[4b,8] The XRD patterns therefore indicate that the pore structure of the SBA-15 silica templates is replicated in the carbons. The overall picture that emerges from the low-angle region of the XRD patterns is that carbons prepared at 900 and 950 °C exhibit good mesostructural ordering, whereas the sample prepared at 1000 °C is relatively less well-ordered. However, it is noteworthy that, even at a CVD temperature of 1000 °C, the XRD pattern of the resulting carbon (RCMK3-100-1000) exhibits low-angle peaks, implying the presence of some mesostructural ordering.

Apart from the low-angle peaks, the wide-angle region of the XRD patterns (inset of Figure 3A) exhibit a high-intensity diffraction peak at $2\theta = 26.2°$ and two additional peaks at $2\theta = 43.4°$ and 54.6° that are ascribed to (002), (101), and (004) diffractions, respectively, of graphitic carbon. The intensity of the wide-angle "graphitic carbon" peaks increases at higher CVD temperatures. In particular, the (002) peak shows a significant increase in intensity for the carbon prepared at 1000 °C, and the (101) and (004) peaks are well-resolved. This suggests an increase in graphitic ordering for carbons prepared at higher CVD temperatures. The d_{002} spacing obtained from the (002) peaks decreases gradually from 3.42 Å for the sample prepared at 900 °C to 3.38 and 3.36 Å for the samples prepared at 950 and 1000 °C, respectively. The d_{002} spacing therefore approaches that of

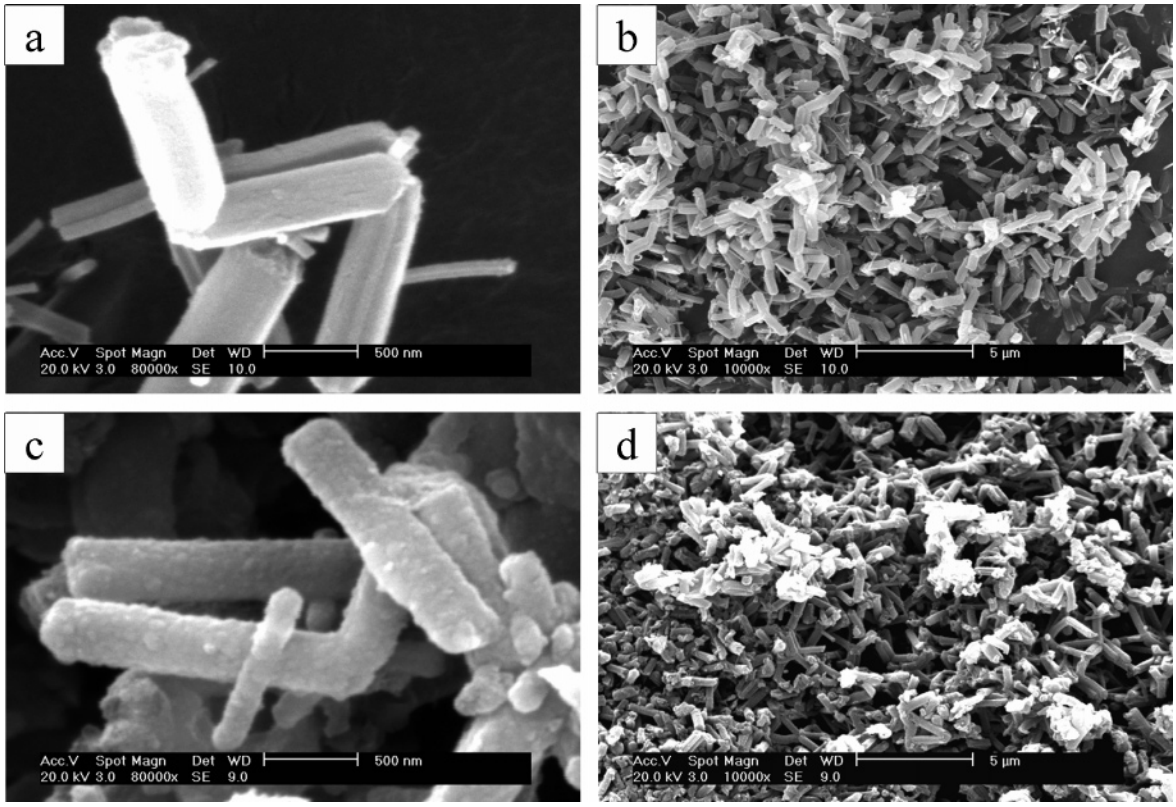

Figure 2. Representative SEM images for (a,b) mesoporous silica SBA-15 rods (sample RSBA15-100) and (c,d) mesoporous carbon rods nanocast from the silica rods via CVD at 1000 °C (sample RCMK3-100-1000).

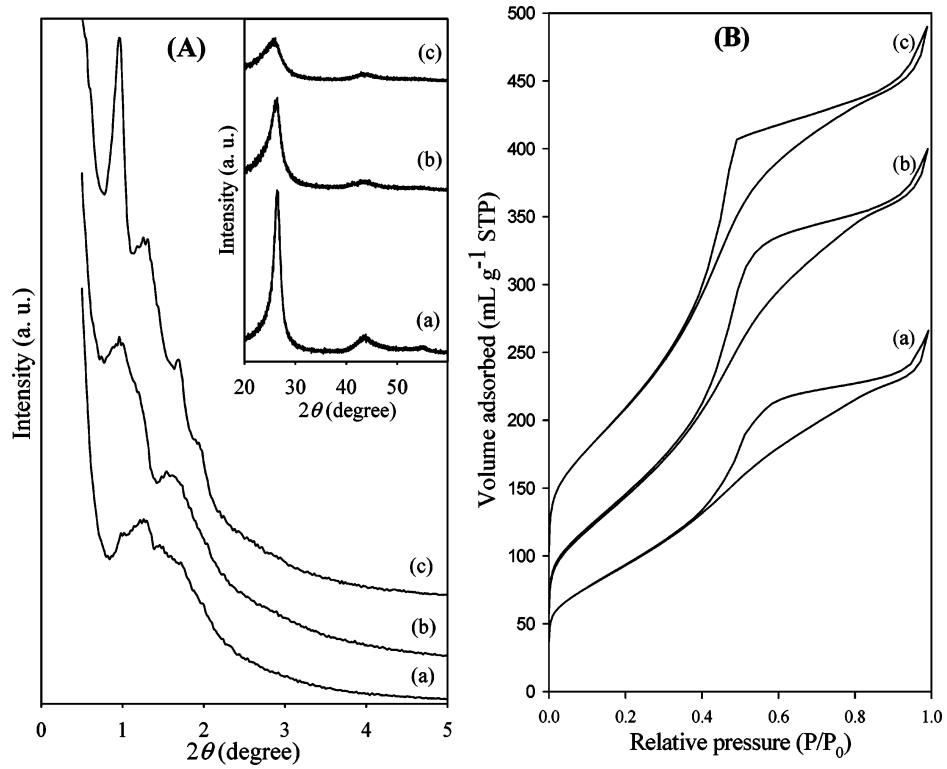

Figure 3. (A) Powder XRD patterns and (B) nitrogen sorption isotherms of mesoporous carbon rods nanocast from SBA-15 silica rods at various CVD temperatures: (a) 1000 °C (RCMK3-100-1000), (b) 950 °C (RCMK3-100-950), (c) 900 °C (RCMK3-100-900). The inset in A shows the wide-angle region of the XRD patterns. For clarity, isotherm c in B is offset (*y* axis) by 40.

ideal graphite ($d_{002} = 3.35$ Å) for carbons prepared at higher CVD temperatures. This provides further evidence that higher levels of graphitization are generated for carbons prepared at 950 and 1000 °C.

The carbons exhibit nitrogen sorption isotherms (Figure 3B) typical of well-ordered CMK-3 mesoporous carbons.[4b] As shown in Table 1, both the surface area and the pore volume of the graphitic mesoporous carbon materials de-

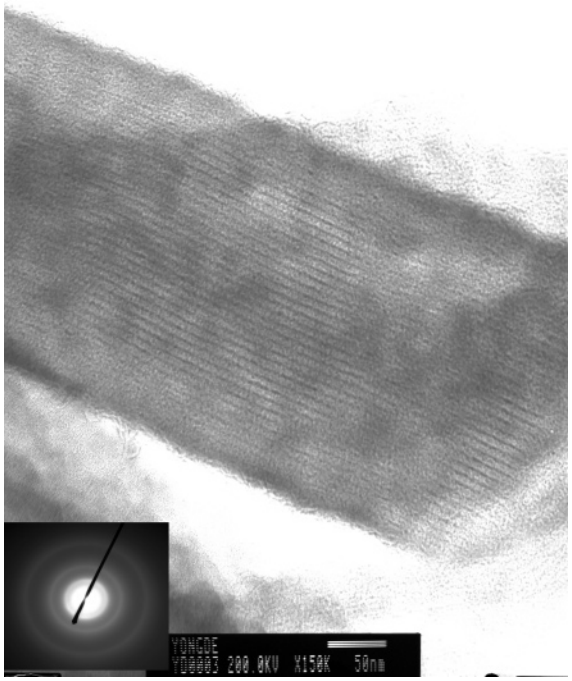

Figure 4. Representative TEM image of a mesoporous carbon rod prepared at a CVD temperature of 950 °C (sample RCMK3-100-950). The inset shows the corresponding SAED pattern.

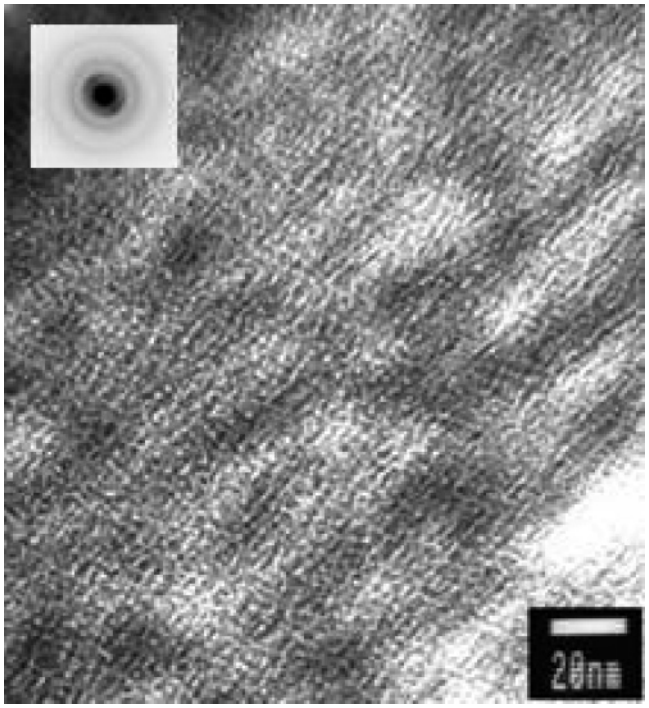

Figure 5. Representative TEM image of a mesoporous carbon obtained at a CVD temperature of 1000 °C (sample RCMK3-100-1000). The inset shows the corresponding SAED pattern.

crease gradually as the extent of graphitization increases for samples prepared at higher CVD temperatures. The mesoporous carbons did not present any microporosity, which is consistent with the nongeneration of secondary porosity during the CVD nanocasting process.[8,16] It is noteworthy that variations in the CVD temperature had little effect on the pore diameter (ca. 3.2 nm) of the mesoporous carbons. Given the variation in basal spacing of the carbons discussed above (i.e, lower spacing at higher CVD temperatures), the unchanging pore size suggests that the pore wall thickness varies according to the CVD temperature. A rough estimate indicates pore wall thicknesses of ca. 7.3, 6.9, and 5 nm for carbons prepared at 900, 950, and 1000 °C, respectively; the wall thickness decreases at higher CVD temperatures. This is consistent with the fact that lower amounts of carbon are deposited in the silica template at higher CVD temperatures.[8,16,18,19]

The SEM images in Figure 2 show that the rod morphology (and particle size) of the SBA-15 templates (Figure 2a,b) is replicated in the mesoporous carbons (Figure 2c,d). The rod particle morphology was also evidenced by TEM as shown in Figure 4. The TEM image (for sample RCMK-3-100-950, prepared at CVD temperature of 950 °C) shows that the rods contain well-ordered pore channels, which is consistent with the corresponding XRD pattern (Figure 3A, pattern b). The selected-area electron diffraction (SAED) pattern in Figure 4 (inset) shows diffraction rings that confirm the formation of semicrystalline (i.e., partially graphitic) pore walls. A representative TEM image for sample RCMK3-100-1000, which was prepared at a CVD temperature of 1000 °C, is shown in Figure 5. The image provides evidence for the presence of some pore channel ordering, but at a lower level compared to the sample prepared at 950 °C (Figure 4). The SAED pattern (inset of Figure 5) shows diffraction rings that are consistent with the presence of graphitic domains. The TEM image therefore confirms the presence of mesostructural ordering in the 1000 °C sample despite the high level of graphitization.

Judging from the effect of the CVD temperature on the structural ordering and graphitization of carbons nanocast from SBA-15 silica template prepared at 100 °C, a temperature of 950 °C was chosen to nanocast carbons from the other SBA-15 silica templates (prepared by crystallization at 40, 70, or 130 °C) in an attempt to vary the pore size and morphology of the carbons. The remainder of this report is therefore concerned with variations in porosity and morphology that result from the use of different SBA-15 silica templates.

3.3. Porosity of Mesoporous Carbon Nanocast from Various SBA-15 Silica Templates. A CVD temperature of 950 °C was used to nanocast carbons from various SBA-15 silica templates (i.e., SBA-15 silicas prepared at crystallization temperatures of 40, 70, 100, or 130 °C). The resulting carbons, with the exception of sample RCMK3-40-950, exhibit type IV nitrogen sorption isotherms (Figure 6A) with a well-developed capillary condensation step into mesopores in the partial pressure range of 0.35−0.8, indicating good mesostructural ordering. Sample RCMK3-40-950 (prepared from the 40 °C silica template), on the other hand, displays an isotherm that suggests the presence of micropores and/or small mesopores. Figure 6B shows that the carbons have relatively narrow pore size distributions. It is interesting to note that the maximum of the pore size distribution (i.e., average pore diameter) of the carbons largely depends on the silica template. The pore size is larger for carbons

(18) Fuertes, A. B.; Nevskaia, D. M. *J. Mater. Chem.* **2003**, *13*, 1843.
(19) Yang, Z.; Xia, Y. D.; Mokaya, R. *Microporous Mesoporous Mater.* **2005**, *86*, 69.

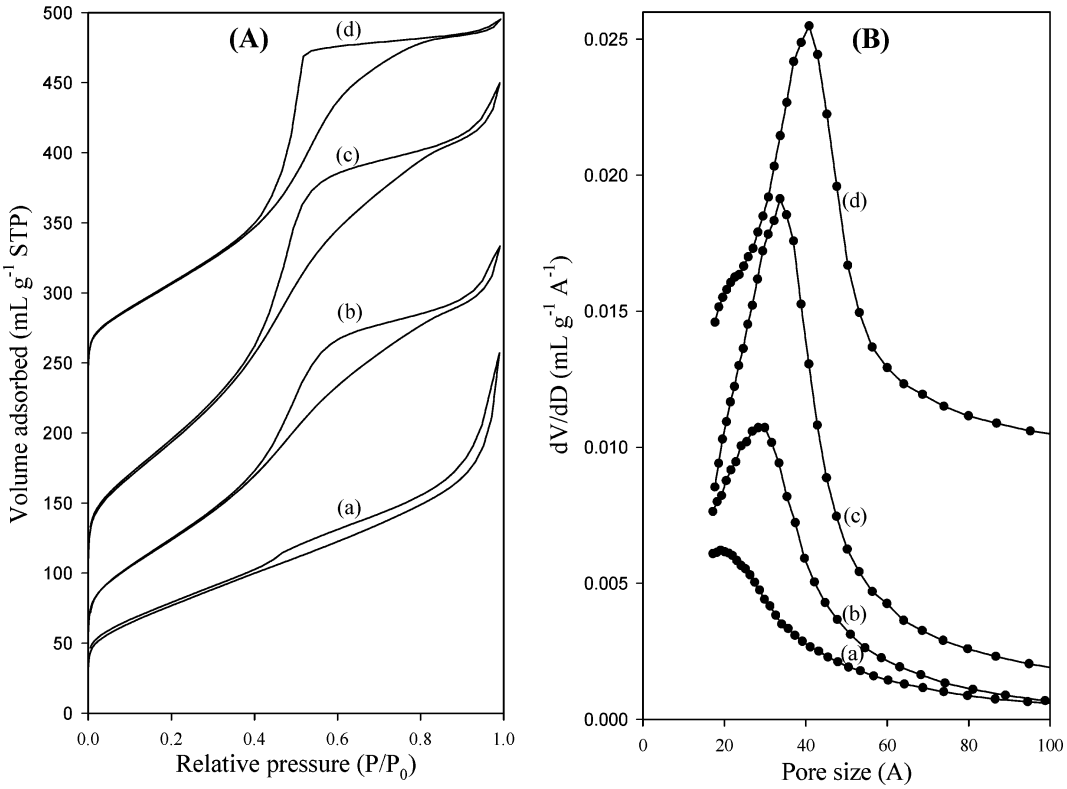

Figure 6. (A) Nitrogen sorption isotherms and (B) pore size distribution curves of mesoporous carbon nanorods nanocast from various mesoporous silica SBA-15 templates: (a) RCMK3-40-950, (b) RCMK3-70-950, (c) RCMK3-100-950, (d) RCMK3-130-950. For clarity, isotherms c and d are offset (*y* axis) by 50 and 200, respectively, and curve d is offset (*y* axis) by 0.01.

nanocast from silicas prepared at higher crystallization temperatures. The pore size of the carbons was tunable between 2 and 4.5 nm depending on the nature of the SBA-15 silica template. As shown in Table 1, the overall porosity (surface area and pore volume) of the carbons is influenced by the nature of the silica template. In general, the textural properties are high for carbons nanocast from silica templates that themselves have high surface areas and pore volumes. Sample RCMK3-100-950, which was nanocast from silica prepared at 100 °C (RSBA15-100), exhibits the highest surface area and pore volume.

The powder XRD patterns of the carbons nanocast from various SBA-15 silica templates are shown in Figure 7. The patterns exhibit graphitic carbon peaks: the (002) diffraction peak at $2\theta = 26.2°$ and at least one additional (101) diffraction peak at $2\theta = 43.4°$. The intensities of the graphitic peaks indicate significant and comparable extents of graphitization. The nature of the SBA-15 silica does not appear to affect the extent of graphitization. The structural ordering of the mesoporous carbons was influenced by the nature of the SBA-15 silica templates as shown by the low-angle XRD patterns in Figure 7 (inset). The XRD patterns indicate that sample RCMK3-40-950, which was prepared from the 40 °C SBA-15 silica template, had a lower level of structural ordering compared to the other carbons—this observation is consistent with the isotherms and PSD curves in Figure 6. However, the overall picture that emerges is that, despite the variations in the extent of long-range structural ordering, low-angle XRD peaks indicative of pore channel ordering were observed for all of the carbons nanocast from the various silica templates.

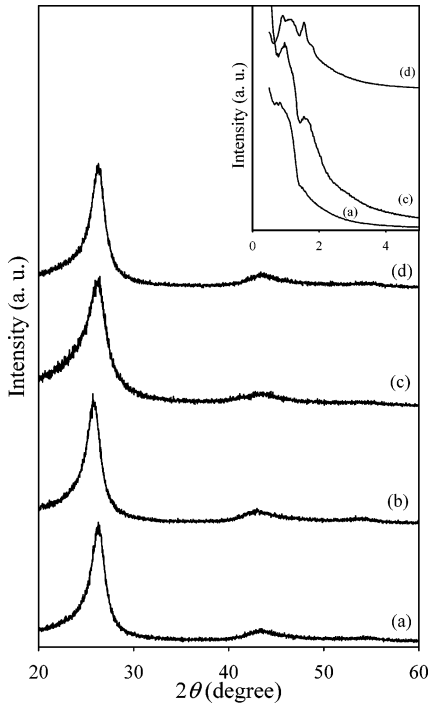

Figure 7. Powder XRD patterns of mesoporous carbon rods nanocast from various mesoporous silica SBA-15 templates: (a) RCMK3-40-950, (b) RCMK3-70-950, (c) RCMK3-100-950, (d) RCMK3-130-950.

3.4. Morphology of Mesoporous Carbon Nanocast from Various SBA-15 Silica Templates. Figure 8 shows SEM images of the mesoporous carbons prepared from the various silica templates. Well-formed rods are observed for all of the carbons as the predominant particle morphology, which was confirmed by low-magnification SEM images (Support-

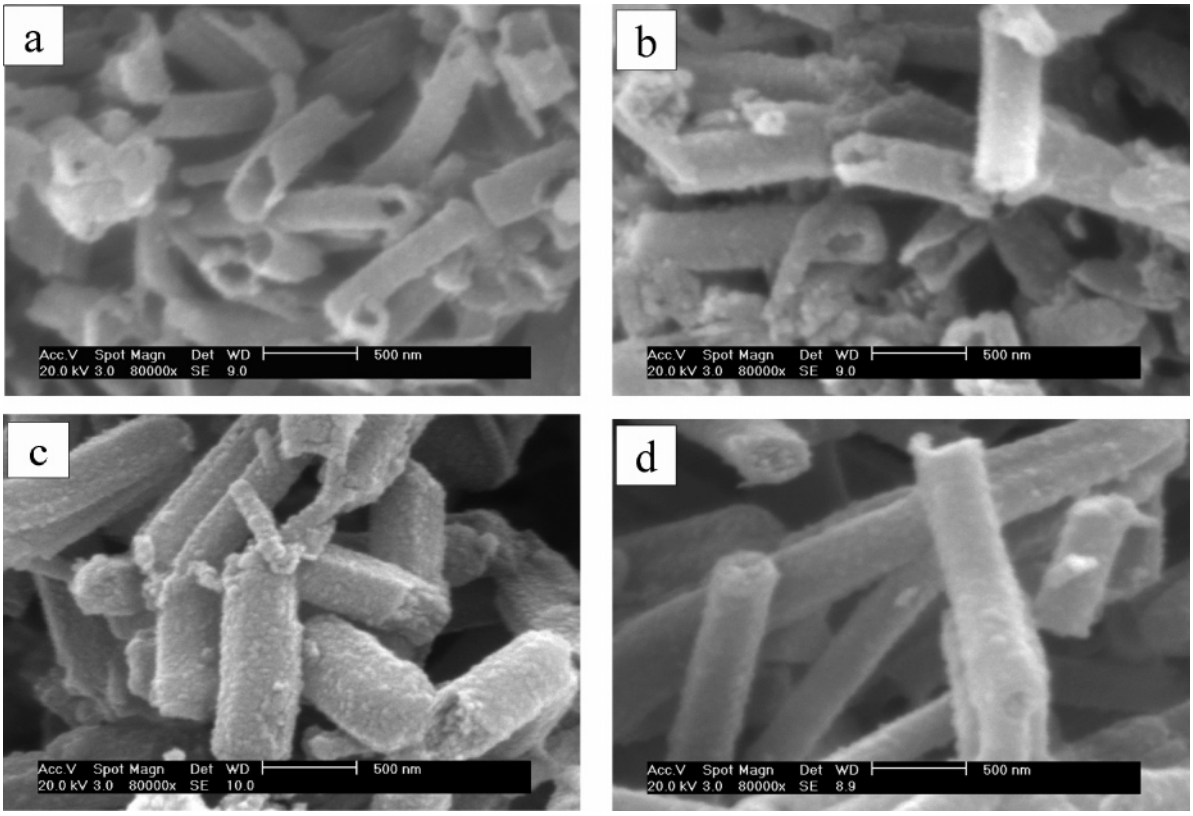

Figure 8. Representative SEM images of graphitic mesoporous carbon materials nanocast using various mesoporous silica SBA-15 rods as templates at a CVD temperature of 950 °C: (a) RCMK3-40-950, (b) RCMK3-70-950, (c) RCMK3-100-950, and (d) RCMK3-130-950.

ing Information, Figure S1). However, it is interesting to note that samples RCMK3-40-950 and RCMK3-70-950, which were nanocast from SBA-15 rods synthesized at lower crystallization temperatures (40 and 70 °C, respectively), exhibit hollow rods (tubules) whereas samples RCMK3-100-950 and RCMK3-130-950, which were nanocast from SBA-15 rods synthesized at higher crystallization temperatures (100 and 130 °C, respectively), have solid-core rods (more SEM images are shown in Figure S2 of the Supporting Information). In particular, virtually all of the particles of sample RCMK3-40-950 are hollow rods (tubules). This is an interesting observation that suggests that the pore size of the silica template directs the morphology of the carbons toward the formation of hollow particles.

We believe that the formation of hollow rods (tubules) is related to the smaller pore size of the relevant SBA-15 silica templates. The role that the pore size of the silica template plays in the formation of hollow rods can be explained as follows: During the CVD process, the carbon precursor (acetonitrile) is initially in contact with the surface of the SBA-15 template rods before diffusing into the interior of the silica rods. The high CVD temperature (950 °C) accelerates carbonization of the acetonitrile once it is in contact with the SBA-15 silica rods. If the pore diameter of the SBA-15 silica template is small, the carbonization process (i.e., deposition of carbon on the surface or near the surface region of silica rods) can quickly block the pore channels and hinder diffusion of the acetonitrile into the core of the silica rods. In such a scenario, narrow pore channels are more susceptible to pore blocking by the deposited carbon (during CVD) compared to wider pores. This would form a carbon/silica composite that is primarily composed of a carbon-rich outer shell surrounding a relatively pure silica inner core. Removal of the silica by HF etching results in hollow carbon rods (Figure 8a). If, on the other hand, the pore diameter of the SBA-15 silica rods is large, the pores will be less susceptible to blocking. In the absence of pore blocking (i.e., larger-pore silica template), the acetonitrile will diffuse deep into the core of the silica rods to form uniform carbon/silica composites. Removal of the silica will yield solid-core carbon rods as shown in Figure 8c,d.

The formation of the hollow carbon rods (nanotubules) was confirmed by TEM as shown in Figure 9. The TEM images of sample RCMK3-40-950, which was prepared from the small-pore 40 °C SBA-15 silica template, clearly show the presence of nanotubules. The TEM images also confirm that the outer shells of the nanotubules are mesostructured with wormhole-type pore channel ordering. We note that the mesostructural ordering observed in the outer shells of the nanotubules is consistent with the porosity data (Table 1 and Figure 6) and XRD patterns (Figure 7) of sample RCMK3-40-950. The SAED pattern (inset of Figure 9) shows diffraction rings, which is an indication of a significant level of graphitization in the mesoporous carbon.

3.5. Carbon Yield of Mesoporous Carbons Nanocast by Various SBA-15 Silica Templates. Two important considerations in the formation of the mesoporous carbons, and in particular the nanotubules, are the removal of silica during etching in hydrofluoric (HF) acid and the carbon yield. We performed thermogravimetric analysis (TGA) of as-synthesized and HF-treated carbon materials to assess the efficiency of silica removal. The TGA data also provided

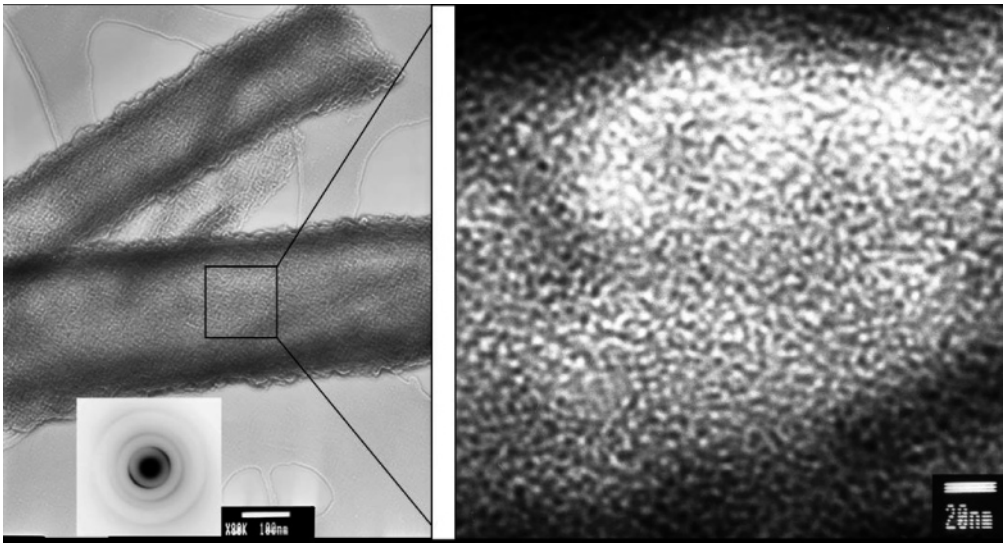

Figure 9. Representative TEM images of mesoporous carbon nanotubules (sample RCMK3-40-950). The carbon was nanocast at a CVD temperature of 950 °C from SBA-15 silica template prepared by crystallization at 40 °C. The inset shows the corresponding SAED pattern.

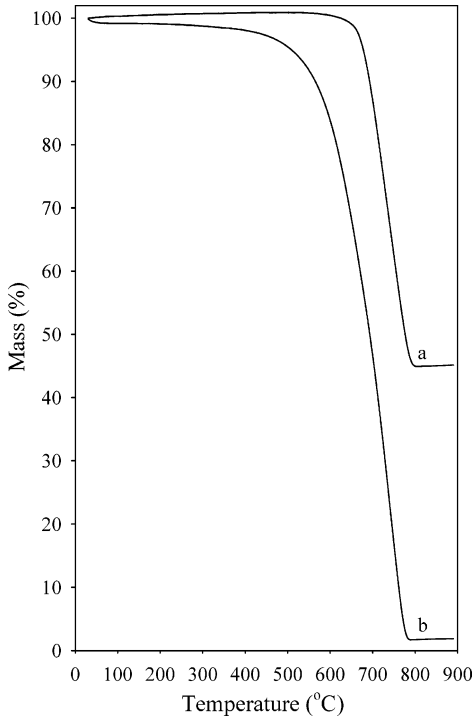

Figure 10. Thermogravimetric analysis of (a) as-synthesized and (b) silica-etched (HF-treated) RCMK3-70-950 samples.

information on the carbon yield. Figure 10 shows TGA curves for as-synthesized and HF-treated RCMK3-70-950 samples. The total mass loss, at 850 °C, for the as-synthesized sample (curve a) was 54.9%. This suggests that the silica/carbon composite contained 54.9 wt % carbon. The TGA curve of the HF-treated sample (curve b) shows a mass residue of <1.5 wt %, which confirms that the carbon material was virtually silica-free. The carbon yield for sample RCMK3-70-950 is therefore at least 1.1 g of carbon per gram of silica template (i.e., 1.1 g of C/g of silica).

The formation of hollow nanotubules should be accompanied by lower carbon yields as only the outer part of the silica rods is involved in the inverse replication (i.e., infiltration with the carbon precursor) process that generates mesoporous carbon. TGA analysis (Supporting Information Figure S3) indicated that the carbon content, in as-synthesized carbon/silica composites, was lower for hollow nanotubules (30.7 and 54.9 wt % for samples RCMK3-40-950 and RMCK3-70-950, respectively) compared to solid rods (57.4 wt % for RMCK3-130-950). The carbon content corresponds to carbon yields (grams of C per gram of silica) of ca. 0.44 for RCMK3-40-950 and 1.35 for RMCK3-130-950. The carbon yields are therefore lower for nanotubules (0.44−1.1 g of C/g of silica) compared to solid rods (1.35 g of C/g of silica). This is consistent with our proposed mechanism for the formation of hollow carbon nanotubules.[8] Moreover, the higher carbon yield for RCMK3-70-950 (1.1 g of C/g of silica) compared to RCMK3-40-950 (0.44 g of C/g of silica) is consistent with the fact that the nanotubules of the former have thicker shells (Figure 8 and Supporting Information Figure S2). Overall, the TGA studies highlight the importance of pore size (of the silica template) in directing the morphology of the mesoporous carbons toward nanotubules rather than nanorods.

4. Conclusions

In summary, we have shown that structurally well-ordered graphitic mesoporous carbon nanorods and nanotubules with tunable pore size can be nanocast using mesoporous silica SBA-15 rods as templates via a simple chemical vapor deposition route. We have demonstrated the nanocasting of graphitic mesoporous carbons with a tunable pore size and shown that the morphology of the carbons can be tailored to hollow rods (tubules) or solid rods simply by varying the pore size of the mesoporous silica templates. We believe that the general principles demonstrated here for the control of morphology are not limited to nanorods or nanotubules; other types of hollow particles (e.g., hollow spheres and cubes) can also be achieved by choice of the pore size of silica templates. To the best of our knowledge, this is the first successful attempt to control both the morphology and the pore size of mesoporous carbons that exhibit graphitic characteristics. Furthermore, we have succeeded in demonstrating a new concept in which the pore size of the silica template plays a key role in directing the morphology of

mesoporous carbon toward hollow nanotubules rather than solid rods. Structurally well-ordered carbon materials that exhibit graphitic character, tunable pore size, and rod or tubular morphology are likely to find use in a variety of applications including in gas storage and as electrode materials or catalyst supports.

Acknowledgment. This work was funded by the EPSRC.

Supporting Information Available: Three additional figures; low magnification SEM images of mesoporous carbon rods, SEM images of mesoporous carbon nanorods and nanotubules and TGA curves showing the dependence of carbon yield on the pore size of the silica template. This information is available free of charge via the Internet at http://pubs.acs.org.

CM0522634